Determination of Thermal Properties of Unsmooth Si Nanowires

Shixian Liu(刘世贤), Alexander A. Barinov*, Fei Yin(闫菲), and Vladimir I. Khvesyuk

Department of Thermophysics, Bauman Moscow State Technical University, Moscow 105005, Russian Federation

(Received 7 October 2023; accepted manuscript online 24 November 2023)

We estimate the thermal properties of unsmooth Si nanowires, considering key factors such as size (diameter), surface texture (roughness) and quantum size effects (phonon states) at different temperatures. For nanowires with a diameter of less than 20 nm, we highlight the importance of quantum size effects in heat capacity calculations, using dispersion relations derived from the modified frequency equation for the elasticity of a rod. The thermal conductivities of nanowires with diameters of 37, 56, and 115 nm are predicted using the Fuchs–Sondheimer model and Soffer's specular parameter. Notably, the roughness parameters are chosen to reflect the technological characteristics of the real surfaces. Our findings reveal that surface texture plays a significant role in thermal conductivity, particularly in the realm of ballistic heat transfer within nanowires. This study provides practical recommendations for developing new thermal management materials.

DOI: 10.1088/0256-307X/41/1/016301

Research of heat transfer in low-dimensional systems is attracting increasing interest owing to the special thermal properties that emerge at the nanoscale, challenging the applicability of classical heat conduction laws, such as Fourier's law, which hold for macroscopic systems. Extensive research has shown unique thermophysical properties of silicon nanowires (SiNWs). Earlier experimental studies[1] indicated that the thermal conductivity of SiNWs is approximately two orders of magnitude lower than that of their bulk counterparts. In addition, as the diameter of SiNWs shrinks, their thermal conductivity decreases. Experiments have shown that thermal conductivity peaks occur at temperatures of approximately 210, 160, and 130 K for SiNWs with diameters of 37, 56, and 115 nm, respectively. This behavior contrasts with macroscopic silicon, where the peak thermal conductivity occurs at approximately 25 K. The key factor behind this discrepancy is the heightened importance of phonon boundary scattering over phonon–phonon scattering as the diameter of nanowires decreases.

Thermal conductivity measurements for SiNWs have also been conducted by varying the size (diameter) and surface roughness.[2] The results revealed that the surface roughness significantly affects the thermal conductivity: higher roughness correlates with lower conductivity. The surface texture affects the scattering of phonons at boundaries, which is essential for thermal conduction. High-resolution TEM images were analyzed using spectroscopic methods to accurately determine the surface roughness.[3] Three roughness parameters, i.e., root mean square, correlation length, and power spectrum, were measured, and their relationships as well as their effects on thermal conductivity were analyzed. The data show that the surface roughness has a more pronounced impact on the thermal conductivity of SiNWs than the diameter does.

Moreover, the phonon density of states in nanowires deviates from that in bulk materials (massive rods) owing to quantum size effects. Pochhammer's 1876 work provided solutions, in the form of transcendental frequency equations, to elasticity equations[4] for tension and bending waves in infinitely long cylindrical rods with free surfaces. The complex branching of these equations yields relationships among frequency, wave vector, phase velocity, and group velocity, which are necessary for calculating thermophysical properties. While several numerical methods have been developed to approximate the branches of Pochhammer's equations for different wave modes,[5,6] these methods often result in rough approximations and sometimes lack solutions. In the past decade, these elastic dispersion equations have been revisited to obtain the thermophysical properties of phonons in low-dimensional structures.[7,8]

In this Letter, we present a modern numerical algorithm to solve the phonon dispersion relations in nanowires and, for the first time, determine the density of states for confined phonons in SiNWs. Our calculations reveal that for SiNWs with diameters smaller than 20 nm, quantum confinement plays a significant role in the phonon density of states. For SiNWs larger than 20 nm in diameter, using the bulk density of states obtained from first principles proves to be sufficiently accurate.

A common approach to consider the effects of size on thermal conductivity in nanowires employs the Fuchs–Sondheimer model,[9] which solves the Boltzmann transport equation for confined structures such as rods or films and yields the F function, an expression indicating how the mean free path in a confined structure is reduced compared with that in a bulk sample.[10] Other methodologies, such as the Monte Carlo method,[11,12] nonequilibrium molecular dynamics (NEMD) simulations,[13–16] mathematical

*Corresponding author. Email: barinov@bmstu.ru
© 2024 Chinese Physical Society

modeling[17,18] and the nonequilibrium Green's function (NEGF) method,[19] are also used for calculating thermal conductivity but come with their own limitations and difficulties when applied to confined structures and when wave effects are considered.

The surface texture of SiNWs can vary significantly depending on the fabrication technique employed. Experimental evidence also confirms that this surface topography significantly affects the thermophysical properties of the nanowires.[2,3] A major problem is to accurately incorporate the complex surface texture of these real-world rough boundaries into our models. In this work, we compare the classical mathematical model for roughness with actual surface data,[2,3] thus establishing a more optimized model for calculating thermal conductivity.

Thus, when studying the thermophysical properties of nanowires, several key factors must be considered: the influence of quantum confinement on phonon dispersion, the influence of size constraints on phonon diffusion, the impact the real surface texture (roughness) on phonon boundary scattering and temperature variations.

The elastic wave equation[20,21] can be written in vector form as

$$\frac{\partial^2 \boldsymbol{u}}{\partial t^2} = c_{\mathrm{T}}^2 \nabla^2 \boldsymbol{u} + (c_{\mathrm{L}}^2 - c_{\mathrm{T}}^2)\nabla(\nabla \cdot \boldsymbol{u}), \tag{1}$$

where $\boldsymbol{u}$ is the displacement vector, $c_{\mathrm{L}} = (\lambda + 2\mu)/\rho$ and $c_{\mathrm{T}} = \mu/\rho$ are the velocities of longitudinal and transverse acoustic waves, λ and μ are the Lamé constants characterizing the elastic properties of the medium, ρ is the density, and t denotes the time.

As shown in Fig. 1, there are three fundamental elastic waves in an infinite rod. Torsional waves involve only circumferential displacement, which is independent of angle θ. Longitudinal waves are axially symmetric waves characterized by the presence of displacement components in both the radial and axial directions. Flexural waves we will examine in detail in the following involve motions that depend on both θ and z.

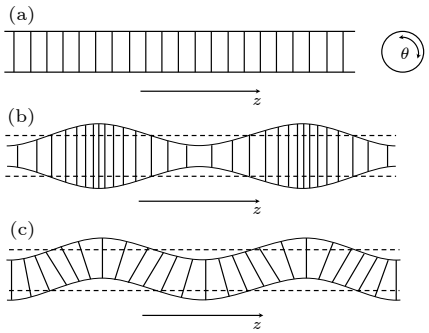

Fig. 1. Schematic diagram of elastic wave displacement in a rod: (a) torsional wave, (b) longitudinal wave, and (c) flexural wave.

Under the assumption of unstressed boundary conditions on the free surface, the following frequency equations can be obtained by derivation[21–23] of Eq. (1) for the three fundamental types of waves.

Torsional waves:

$$k_{\mathrm{T}}R \cdot J_0(k_{\mathrm{T}}R) - 2J_1(k_{\mathrm{T}}R) = 0. \tag{2}$$

Longitudinal waves:

$$(k^2 - k_{\mathrm{T}}^2)^2 \frac{(k_{\mathrm{L}}R)J_0(k_{\mathrm{L}}R)}{J_1(k_{\mathrm{L}}R)} + 4k^2k_{\mathrm{L}}^2 \frac{(k_{\mathrm{T}}R)J_0(k_{\mathrm{T}}R)}{J_1(k_{\mathrm{T}}R)} = 2k_{\mathrm{L}}^2(k^2 + k_{\mathrm{T}}^2). \tag{3}$$

Flexural waves:

$$J_1(\alpha)J_1^2(\beta)[f_1\Psi_\beta^2 + f_2\Psi_\alpha\Psi_\beta + f_3\Psi_\beta + f_4\Psi_\alpha + f_5] = 0, \tag{4}$$

with

$$f_1 = 2(\beta^2 - \xi^2)^2, \quad f_2 = 2\beta^2(5\xi^2 + \beta^2),$$
$$f_3 = \beta^6 - 10\beta^4 - 2\beta^4\xi^2 + 2\beta^2\xi^2 + \beta^2\xi^4 - 4\xi^4,$$
$$f_4 = 2\beta^2(2\beta^2\xi^2 - \beta^2 - 9\xi^2),$$
$$f_5 = \beta^2(-\beta^4 + 8\beta^2 - 2\beta^2\xi^2 + 8\xi^2 - \xi^4),$$

where $\alpha = k_{\mathrm{L}}R$, $\beta = k_{\mathrm{T}}R$ and $\xi = kR$ are dimensionless wave numbers, $\Psi_\alpha = \alpha J_0(\alpha)/J_1(\alpha)$ and $\Psi_\beta = \beta J_0(\beta)/J_1(\beta)$ are auxiliary functions, J_0 and J_1 are Bessel functions of the first kind.

The elastic dispersion relation is obtained using the following equation:

$$\omega_{\mathrm{el}}^2 = c_{\mathrm{T}}^2(k^2 + k_{\mathrm{T}}^2) = c_{\mathrm{L}}^2(k^2 + k_{\mathrm{L}}^2). \tag{5}$$

It is evident from dispersion relation (5) that k_{T} and k_{L} can be either real or imaginary,

$$\begin{aligned} &k_{\mathrm{T}} \text{ and } k_{\mathrm{L}} \text{ real}, \quad \omega_{\mathrm{el}} \geq c_{\mathrm{L}}k \\ &k_{\mathrm{T}} \text{ real}, \quad k_{\mathrm{L}} \text{ imaginary}, \quad c_{\mathrm{T}} \leq \omega_{\mathrm{el}} < c_{\mathrm{L}}k \\ &k_{\mathrm{T}} \text{ and } k_{\mathrm{L}} \text{ imaginary}, \quad \omega_{\mathrm{el}} \leq c_{\mathrm{T}}k. \end{aligned} \tag{6}$$

Therefore, in the imaginary region, we need to rewrite Eqs. (2)–(4) using the following equations:

$$I_n(x) = i^{-n}J_n(ix), \tag{7}$$

where I_n is a modified Bessel function of the first kind.

We have proposed a unique numerical algorithm and the corresponding code that we have made publicly available on GitHub (https://github.com/sxliu98/DS-Slover-in-wire). The algorithm numerically solves Eqs. (2)–(7) in MATLAB, utilizing the built-in function fzero to find the roots of nonlinear equations. The algorithm operates in both the real and imaginary regions. We identify the roots of the equations under the minimum wave vector using a traversal method and then solve the equations layer by layer, starting with these initial sets of solutions. The advantages of this approach include greater accuracy compared with previous approximate solutions, which skipped modes, and improved computational efficiency relative to exhaustive methods. The final result is a comprehensive set of elastic dispersion curves we refer to as modes, for the three types of waves in rods.

To accommodate the infinite nature of the elastic dispersion relation, we employ the Born–von Karman boundary condition to account for the lack of periodicity. This condition modifies each dispersive mode as follows:[24]

$$\omega(k) = [\omega_{\mathrm{el}}(k) \cdot \sin(ka/2)]/(ka/2). \tag{8}$$

This method sets to zero the group velocity of the lowest frequency modes at the edge of the Brillouin zone boundary for a symmetric simple cubic lattice. This modification creates an effective standing wave within each lattice cell for the lowest-frequency modes, enabling us to use the elastic dispersion relations for rods as approximations for the phonon dispersion relations in nanowires.

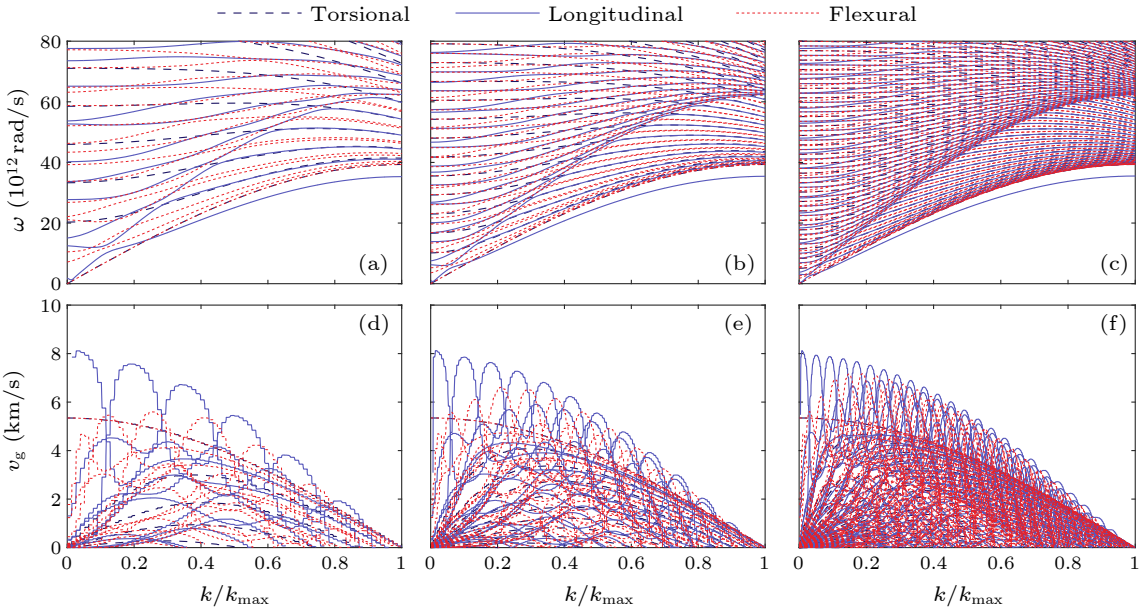

Fig. 2. Dispersion relations for SiNWs with diameters of (a) 2.7, (b) 5.4, and (c) 10.8 nm. Group velocities for SiNWs with diameters of (d) 2.7, (e) 5.4, and (f) 10.8 nm.

For SiNWs with diameters of 2.7, 5.4, and 10.8 nm, the dispersion relations are depicted in Figs. 2(a), 2(b), and 2(c), respectively. The group velocity of each mode is defined as the gradient of frequency. For SiNWs with diameters of 2.7, 5.4, and 10.8 nm, the group velocity is depicted in Figs. 2(d), 2(e), and 2(f), respectively.

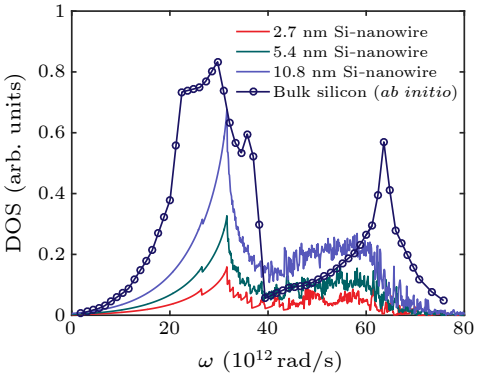

Fig. 3. DOSs of confined phonons in SiNWs and phonons in bulk silicon.

Next, we determine the phonon density of states (DOS) to estimate the impact of quantum size effects on phonon states in confined structures. Using the dispersion relations, the DOS can be expressed as an integral over the first Brillouin zone,[25]

$$\mathrm{DOS}(\omega) = \sum_s g_s(\omega) = \sum_s \sum_j \int_{\mathrm{BZ}} \frac{dk}{2\pi} \delta(\omega - \omega_j(k)), \quad (9)$$

where s represents different polarizations, j represents different modes, and $\delta(x)$ represents the Dirac delta function. Figure 3 shows the phonon DOS for SiNWs with diameters of 2.7, 5.4, and 10.8 nm calculated using the dispersion curves shown in Figs. 2(a), 2(b), and 2(c), respectively. Additionally, Fig. 3 shows the phonon DOS for bulk silicon obtained from first principles in a local density approximation using soft pseudopotentials and a plane wave basis in Quantum Espresso software.[26] It is evident that as the diameter of the nanowire increases, the phonon DOS gradually approaches that of bulk silicon. Moreover, for diameters of approximately 20 nm and more, the deviation between the phonon DOS of the nanowire and that of bulk silicon becomes negligible.

The phonon heat capacity[27] in SiNWs is determined using the following frequency integration:

$$C_v(T, R) = k_{\mathrm{B}} \sum_s \int_{\omega_{\min,s}}^{\omega_{\max,s}} \left(\frac{\hbar\omega}{k_{\mathrm{B}}T}\right)^2 \overline{n}(\overline{n}+1) \cdot g_s(\omega, R) d\omega, \quad (10)$$

where s denotes the different polarizations, and $\overline{n}$ denotes the Bose–Einstein equilibrium distribution:

$$\overline{n}(\omega, T) = [\exp(\hbar\omega/k_{\mathrm{B}}T) - 1]^{-1}. \quad (11)$$

For SiNWs with diameters of 2.7, 5.4, and 10.8 nm, the heat capacity of confined phonons is illustrated in Fig. 4. The dotted line in Fig. 5 represents the one-dimensional heat capacity calculated using the classical Debye model $C_{1D} \approx \frac{1.736T^{1/2}}{\pi}\sqrt{2k_{\mathrm{B}}^3/\hbar c_0 R}$, with R denoting the diameter of the nanowire.[28] It is evident that the phonon heat capacity for SiNWs exhibiting phonon confinement approaches the one-dimensional heat capacity at low temperatures. This is due to the fact that flexural wave plays

a dominant role and conforms to the $T^{0.5}$ rule. However, when the temperature increases, the phonon vibration intensifies and the heat capacity of the nanowires behaves more like a 3D model and becomes increasingly independent of the nanowire diameter.

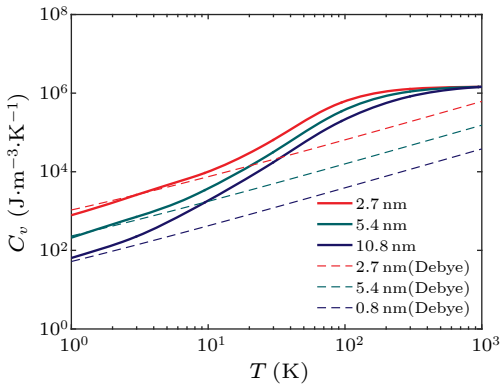

Fig. 4. Heat capacity of confined phonons in SiNWs with diameters of 2.7, 5.4, and 10.8 nm. The dotted line shows the one-dimensional heat capacity based on the Debye model.[28]

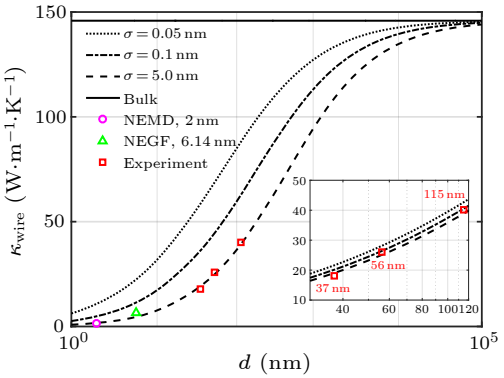

Fig. 5. Thermal conductivity ($\kappa_{\rm wire}$) of SiNWs depending on diameter (d) and rms roughness (σ) at a temperature of 300 K. The squares represent the experimental data,[1] the circle represents the results based on NEMD[14,15] and the triangle represents the results based on the NEGF method.[19]

When the characteristic size of the SiNWs (denoted as d) is smaller than the phonon mean free path, boundary scattering becomes a pivotal factor influencing heat transfer. This phenomenon is called the size effect. By solving the steady-state Boltzmann transport equation devoid of external forces and sources within the relaxation time approximation,[29] a generalized expression for lattice thermal conductivity of nanowires can be derived:

$$\kappa = \frac{1}{3}k_{\rm B}\sum_s \int_{\omega_{{\rm min},s}}^{\omega_{{\rm max},s}} \left(\frac{\hbar\omega}{k_{\rm B}T}\right)^2 \overline{n}(\overline{n}+1) \cdot g_s(\omega)\cdot v^2\tau \cdot F(Kn,\, p)d\omega, \tag{12}$$

where s denotes the different polarizations. $F(Kn,\, p)$ quantifies the reduction, attributable to the size effect, in the free path length in nanowires compared with that in a bulk sample:[10]

$$F(Kn,\, p) = \frac{l_{\rm wire}}{l_{\rm bulk}} = 1 - \frac{12(1-p)^2}{\pi}\sum_{m=1}^{\infty} m p^{m-1} G(Kn,\, m), \tag{13}$$

where

$$G(Kn,\, m) = \int_0^1 \sqrt{1-\xi^2}\int_1^{\infty} \exp\left(-\frac{m\xi t}{Kn}\right)\frac{\sqrt{t^2-1}}{t^4}dtd\xi. \tag{14}$$

Here, the Knudsen number Kn and the specular parameter p are the only factors affecting F. The specular parameter indicates the fraction of phonons that are reflected specularly/diffusely upon interaction with a rough surface. A value of $p = 1$ corresponds to purely specular scattering, whereas $p = 0$ corresponds to completely diffuse reflection. The Knudsen number is associated with the wire diameter, and parameter p pertains to the roughness of the surface.

Assuming an infinite correlation length, Soffer[30] derived a straightforward expression for the specular parameter as a function of the rms roughness σ:

$$p(k,\, \sigma,\, \theta) = \exp(-4k^2\sigma^2\cos^2\theta), \tag{15}$$

where k denotes the phonon wave number and θ represents the angle between the phonon momentum and the normal to the idealized smooth surface boundary. In fact, σ is the rms roughness of the vertical deviation of the true contour from the average smooth surface.

Phonons in a crystal experience scattering through various mechanisms,[31] such as phonon–phonon interactions and interactions with lattice impurities. It is noteworthy that scattering involving three or more phonons occurs owing to the anharmonic nature of interatomic forces and the discrete lattice structure. Scattering involving four or more phonons becomes important only at temperatures considerably above the Debye temperature for silicon, which is 645 K.[32] This is generally irrelevant for practical applications, as these temperatures exceed the operational range of most electronic devices.

Three-phonon scattering processes are primarily categorized into normal (N) and umklapp (U) processes.[33] In these interactions, either two phonons combine to create a third phonon, or a single phonon decays into two. The U-process is unique in that momentum is not conserved; the discrepancy in wave vectors leads to an inverse lattice vector. In the N-process, both momentum and energy are conserved. While normal phonon scattering does not contribute to resistance, it is essential for calculating the thermal conductivity in the Callaway model.

All these scattering mechanisms contribute to energy exchange between lattice waves. Because each scattering process is independent, the overall scattering time τ can be determined using Matthiessen's rule[34] given as follows:

$$\tau^{-1} = \tau_{\rm N}^{-1} + \tau_{\rm U}^{-1} + \tau_{\rm imp}^{-1}, \tag{16}$$

where $\tau_{\rm N}$ denotes the relaxation time due to phonon–phonon N-process interactions, $\tau_{\rm U}$ denotes the relaxation time due to phonon–phonon U-process interactions, and

$\tau_{\rm imp}$ represents the relaxation time from interactions with lattice impurities.

Many scientists have studied phonon–phonon nonlinear interactions and proposed mathematical expressions.[31–39] After comparing the results obtained by applying these models to bulk silicon, we selected a model that is more consistent with the experimental results,[35] as described in the following.

Morelli *et al.*[37] proposed a model focused solely on U-process interactions. This model employs the dimensionless variable $x = \hbar\omega/k_{\rm B}T$ and is expressed as follows:

$$\tau_{\rm U}^{-1} = \begin{cases} \tau_{\rm T,U}^{-1} = B_{\rm TU}(k_{\rm B}/\hbar)^2 x^2 T^3 \exp(-\theta_{\rm T}/3T), \\ \tau_{\rm L,U}^{-1} = B_{\rm LU}(k_{\rm B}/\hbar)^2 x^2 T^3 \exp(-\theta_{\rm L}/3\,T), \end{cases} \tag{17}$$

where the coefficients $B_{\rm TU}$ and $B_{\rm LU}$ for silicon are 1.0×10^{-19} and $5.5 \times 10^{-20}\,{\rm s}^{-1}{\rm K}^{-3}$, respectively. Additionally, the characteristic temperatures $\theta_{\rm T}$ and $\theta_{\rm L}$ for silicon are 240 and 586 K, respectively.

Herring proposed several formulations depending on the crystal type.[38] Adopting the Asen–Palmer approach,[39] the appropriate equation for longitudinal and transverse phonons for a specific crystallographic material is expressed in terms of the dimensionless variable $x = \hbar\omega/k_{\rm B}T$ as follows:

$$\tau_{\rm N}^{-1} = \begin{cases} \tau_{\rm T,N}^{-1} = B_{\rm TN}(k_{\rm B}/\hbar) x T^5, \\ \tau_{\rm L,N}^{-1} = B_{\rm LN}(k_{\rm B}/\hbar)^2 x^2 T^5, \end{cases} \tag{18}$$

where the coefficients $B_{\rm TN}$ and $B_{\rm LN}$ for silicon are 7.1×10^{-13} and $2.4 \times 10^{-24}\,{\rm s}^{-1}{\rm K}^{-5}$, respectively.

Klemens pioneered the calculation of the intensity of phonon scattering due to isolated defects with masses differing from those of the primary element in an ideal crystal.[40] For such cases, the scattering intensity is represented by

$$\tau_{\rm imp}^{-1} = \frac{V k_{\rm B}^4 \Gamma}{4\pi\hbar^4 v^3} x^4 T^4. \tag{19}$$

For natural silicon, which consists of 92.2% ^{28}Si, 4.7% ^{29}Si, and 3.1% ^{30}Si, the mass-fluctuation parameter is $\Gamma = 2.0 \times 10^{-4}$.[40]

Based on the aforementioned model, we have developed a comprehensive set of programs designed to predict the properties of SiNWs across a wide range of significant parameters, including temperature, diameter, and rms roughness.

We performed calculations to determine the thermal conductivity of SiNWs with different diameters and levels of rms roughness at a constant temperature of 300 K. Figure 5 reveals that as the nanowire diameter increases, the thermal conductivity of SiNWs gradually approaches that of bulk silicon. Moreover, the data show that for a fixed diameter of nanowire, an increase in rms roughness leads to a reduction in thermal conductivity. These observations are in agreement with experimental results.

To validate our model, we compared our predictions with available experimental data. One challenge in this regard is that many general studies on the thermal conductivity of SiNWs, such as the work by Li *et al.*,[1] do not specify surface roughness. However, the studies by Lim *et al.*[3] and Feser *et al.*[2] provided sufficient data on both the diameter and surface roughness of SiNWs produced by various methods. These data points are represented as circles and squares in Fig. 6. We further delineate an area between two lines to ensure that all the experimental points fall within this region.

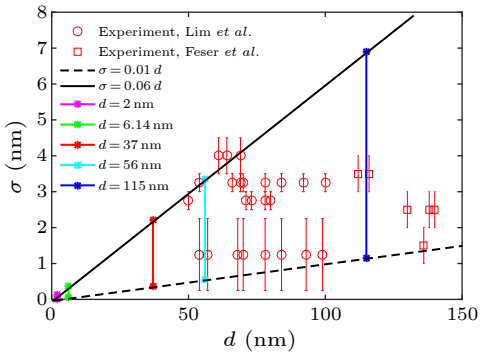

Fig. 6. Relationship between surface roughness and diameter of SiNWs from the experiments of Lim *et al.*[3] and Feser *et al.*[2] The black solid and dotted lines delimit the area containing all the experimental data. The magenta, green, red, cyan, and blue solid lines denote roughness ranges, which are chosen for later comparison.

For SiNWs with diameters of 2, 6.14, 37, 56, and 115 nm, we identify the minimum and maximum values of rms roughness. These ranges are represented by magenta, green, red, cyan, and blue intervals, respectively, in Fig. 6. Utilizing these intervals, we then calculate the thermal conductivity of the SiNWs across a temperature range of 100–350 K, as depicted in Fig. 7.

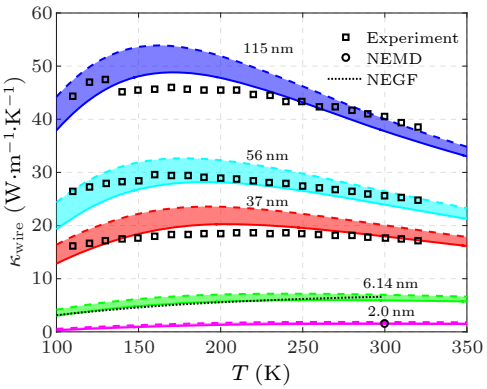

Fig. 7. Thermal conductivity of SiNWs with various diameters. The colored areas correspond to the ranges of nanowire roughness $0.01d < \sigma < 0.06d$ (as shown in Fig. 6). The squares represent the experimental data,[1] the circle represents the results based on NEMD,[14,15] and the dashed line represents the results based on the NEGF method.[19]

As evident from Fig. 7, for SiNWs with a diameter of 115 nm, nearly half of the experimental data points fall within the omitted roughness area. For SiNWs with a diameter of 56 nm, all the experimental data reside in the omitted area of min–max roughness. For SiNWs with a 37 nm diameter, most data points lie outside the specified

interval, although the maximum error remains below 10%. The thermal conductivity of nanowires with diameters of less than 20 nm is only slightly affected by roughness, and our results are in good agreement with those based on other methods.

In summary, we have delved into various factors affecting the thermal properties of SiNWs. We introduce a robust technique to determine the phonon dispersion relation for SiNWs and, for the first time, propose a DOS for confined phonons in SiNWs with diameters of 2.7, 5.4, and 10.8 nm. Our findings highlight the importance of the quantum size effect for diameters below 20 nm. Using the DOS for confined phonons, we calculate their heat capacity in SiNWs. The results reveal that, at temperatures below the Debye temperature, the heat capacity behaves akin to a one-dimensional material, whereas at higher temperatures it resembles that of bulk silicon.

To augment our investigation, we develop a suite of computational tools to evaluate and predict the thermal conductivity of SiNWs, considering variables such as temperature, diameter and rms roughness. We compare the classical roughness models with actual surface data from different studies, which lead to a more optimized model for thermal conductivity calculations. Our results highlight the pivotal role that surface texture plays in nanowire thermal conductivity, making it as influential as the diameter of the confined structure. Hence, both the sample geometry and surface topography must be meticulously specified for effective thermal management in nanostructured systems.

Acknowledgement. S. Liu and F. Yin gratefully acknowledge financial support from the China Scholarship Council.

References

[1] Li D Y, Wu Y Y, Kim P, Shi L, Yang P D, and Majumdar A 2003 *Appl. Phys. Lett.* **83** 2934
[2] Feser J P *et al.* 2012 *J. Appl. Phys.* **112** 114306
[3] Lim J, Hippalgaonkar K, Andrews S C, Majumdar A, and Yang P 2012 *Nano Lett.* **12** 2475
[4] Pochhammer L 1876 *Z. Math.* **81** 324
[5] Holden A N 1951 *Bell Syst. Tech. J.* **30** 956
[6] Pao Y H and Mindlin R D 1960 *J. Appl. Mech.* **27** 513
[7] Khitun A, Balandin A, and Wang K L 1999 *Superlattices Microstruct.* **26** 181
[8] Bifano M F P, Kaul P B, and Prakash V 2010 *Nanotechnology* **21** 235704
[9] Chantrenne P, Barrat J L, Blase X, and Gale J D 2005 *J. Appl. Phys.* **97** 104318
[10] MacDonald D K C 1950 *Proc. R. Soc. Lond. Ser. A* **203** 223
[11] Bera C 2012 *J. Appl. Phys.* **112** 074323
[12] Kukita K and Kamakura Y 2013 *J. Appl. Phys.* **114** 154312
[13] Volz S G and Chen G 1999 *Appl. Phys. Lett.* **75** 2056
[14] Yang N, Zhang G, and Li B 2008 *Nano Lett.* **8** 276
[15] Yang N, Zhang G, and Li B 2010 *Nano Today* **5** 85
[16] Zhu G, Zhao C, Wang X, and Wang J 2021 *Chin. Phys. Lett.* **38** 024401
[17] Wang W Z, Ai Q, Yong S, and Tan H P 2023 *Int. J. Heat Mass Tran.* **206** 123959
[18] He Z, Yuan K, Xiong G, and Wang J 2023 *Chin. Phys. Lett.* **40** 104402
[19] Wang J and Wang J S 2007 *Appl. Phys. Lett.* **90** 241908
[20] Achenbach J 2012 *Wave propagation in Elastic Solids* (Amsterdam: Elsevier) p 236
[21] Bifano M F P and Prakash V 2012 *J. Appl. Phys.* **111** 034319
[22] Zou J and Balandin A 2001 *J. Appl. Phys.* **89** 2932
[23] Au Y T C *et al.* 2006 *Phys. Rev. B* **74** 155317
[24] Tong T, Prasher R and Majumdar A 2007 *Micro and Nanosystems, Parts A and B* (Seattle, WA: ASME) p 631
[25] Pascual-Gutiérrez J A, Murthy J Y, and Viskanta R 2007 *J. Appl. Phys.* **102** 034315
[26] Giannozzi P *et al.* 2017 *J. Phys.: Condens. Matter* **29** 465901
[27] Prasher R, Tong T, and Majumdar A 2008 *Nano Lett.* **8** 99
[28] Kittel C 2005 *Introduction to Solid State Physics* 8th edn (Hoboken: Wiley) p 107
[29] Kaviany M 2008 *Heat Transfer Physics* (Cambridge: Cambridge University Press) p 189
[30] Soffer S B 1967 *J. Appl. Phys.* **38** 1710
[31] Callaway J 1959 *Phys. Rev.* **113** 1046
[32] Barinov A A, Liu B, Khvesyuk V I, and Zhang K 2020 *Phys. At. Nucl.* **83** 1538
[33] Khvesyuk V I and Skryabin A S 2017 *High Temp.* **55** 434
[34] Dugdale J S and Basinski Z S 1967 *Phys. Rev.* **157** 552
[35] Holland M G 1963 *Phys. Rev.* **132** 2461
[36] Ward A and Broido D A 2010 *Phys. Rev. B* **81** 085205
[37] Morelli D T, Heremans J P, and Slack G A 2002 *Phys. Rev. B* **66** 195304
[38] Herring C 1954 *Phys. Rev.* **95** 954
[39] Asen-Palmer M *et al.* 1997 *Phys. Rev. B* **56** 9431
[40] Klemens P G 1955 *Proc. Phys. Soc. A* **68** 1113